RSC Advances

PAPER

View Article Online
View Journal | View Issue

Cite this: *RSC Adv.*, 2021, **11**, 38915

Synthesis and evaluation of ion-imprinted composite membranes of Cr(VI) based on β-diketone functional monomers†

Peng Li, Xin Wang, Guifang Wang, Li Zhao, Yuwen Hong, Xianzhi Hu, Futing Zi and Huiling Cheng *

Using Cr(VI) as the imprinted ions and 2-allyl-1,3-diphenyl-1,3-propanedione (ADPD) (a compound synthesized by independent design) as the functional monomer, a series of chromium ion-imprinted composite membranes (Cr(VI)-IICMs) and corresponding non-imprinted composite membranes (NICMs) were synthesized and tested. The results showed that the Cr(VI)-IICM$_{10}$ membrane prepared under optimal experimental conditions exhibited a high adsorption capacity towards Cr(VI) (Q = 30.35 mg g^{-1}) and a high imprinting factor (α = 2.70). The structural characteristics of Cr(VI)-IICM$_{10}$ and NICM$_{10}$ were investigated using FE-SEM, ATR-FTIR, and BET techniques combined with UV-Vis photometry and inductively coupled plasma emission spectrometry (ICP-OES) to evaluate the adsorption performance and permeation selectivity, while the effect on adsorption permeance of varying the experimental conditions including the solvent type, pH, and temperature was also investigated. The results showed that Cr(VI)-IICM$_{10}$ is a mesoporous material with excellent permeation selectivity, reusability, and favorable pH response, and that its adsorption behavior is in accordance with the Langmuir model and pseudo-first-order kinetics. Thus, Cr(VI)-IICM$_{10}$ shows great potential towards utilization as a "smart membrane" to control the separation and removal of Cr(VI) in wastewater, and also proved a reasonable design of the new functional monomer ADPD.

Received 17th October 2021
Accepted 24th November 2021

DOI: 10.1039/d1ra07678g

rsc.li/rsc-advances

1. Introduction

Statistics from the Ministry of Ecology and Environment of China show that as of 2019, wastewater emissions containing heavy metals (such as Cd, Pb, Cr, and Hg, *etc.*) totaled 120.7 tons. In addition, nearly 16% of soils were chronically polluted with heavy metals, resulting in almost 12 million tons of grain being contaminated every year.[1,2] As a strongly toxic substance, the presence of Cr(VI) in the environment is problematic, as it can easily accumulate in the human body, resulting in liver and kidney damage, gastric ulcers, and cancer (mainly of the lungs and throat).[3–6] At present, wastewater treatment measures for Cr(VI) primarily include chemical precipitation,[7] electrochemical methods,[8,9] ion exchange,[10,11] and membrane separation.[12,13] Although these methods are effective in their own right, each has its own drawbacks.[14–16] For example, chemical precipitation methods may lead to secondary pollution, electrochemical methods tend to be expensive and consume lots of energy, and ion exchange methods often exhibit poor resin stability as these are easily oxidized which may lead to failure. Although membrane separation overcomes some of these drawbacks, offering excellent separation efficiency, environmental friendliness, and ease of operation, it is difficult to achieve the selective separation of metal ions using this method.

To overcome some of these limitations, ion imprinting[17,18] has emerged as a cutting-edge technology based on molecular imprinting techniques. This method adopts various metal ions as templates and binds functional monomers to them. The template ions are then removed by elution, resulting in systems with high selectivity towards these ions. In particular, the use of ion-imprinted composite membranes (IICMs)[19,20] combines the benefits of both ion imprinting and membrane separation. Such membranes are formed by grafting an imprinted layer onto the membrane surface *via in situ* polymerization, allowing cavities of similar shape, size and function to the template ions to be formed at the membrane surface after elution and removal of the template. The resulting IICMs possess excellent separation efficiency, adsorption capacity, and selectivity. Among all ion-imprinted composite membranes (IICMs), the stimuli-responsive membrane is one of the most attractive materials.[22,40] It has the potential to modify its permeation selectivity for metal ions by grafting pH-responsive or temperature-responsive polymers on the substrate membrane. However, the functional monomers currently available for use are almost limited to acrylic acid, methacrylic acid or *N*-

Faculty of Science, Kunming University of Science and Technology, Kunming, China. E-mail: ynchenghl@163.com

† Electronic supplementary information (ESI) available. See DOI: 10.1039/d1ra07678g

isopropylacrylamide. Their enol/ketone group isomerization with changes in polarity or pH in solvents has attracted increasing interest from scientists and has been applied in the field of functional materials.[22] It would be an interesting study to explore a novel stimuli-responsive smart membrane with predetermined affinity for Cr(VI) using β-diketone compounds as functional monomers.

The aim of this study was to synthesize a pH-responsive functional monomer with a β-diketone structure, namely 2-allyl-1,3-diphenylpropane-1,3-dione (ADPD). Its stimulatory responsiveness was verified by UV spectroscopic analysis in solvents of different pH values. A series of Cr(VI) imprinted composite membranes (Cr(VI)-IICM$_{1-11}$) and the corresponding non-imprinted composite membranes (NICM$_{1-11}$) were prepared with the support of commercial nylon filter membranes (Nylon). The optimized Cr(VI)-IICM$_{10}$ was characterized and evaluated based on the results of field emission scanning electron microscopy (FE-SEM), attenuated total reflection-Fourier transform infrared spectroscopy (ATR-FTIR), nitrogen adsorption/desorption analysis and performance testing. Finally, the optimized Cr(VI)-IICM$_{10}$ was successfully used to competitively transport Cr(VI) in a complex system and showed a pH-controlled effect, which is expected to achieve "controlled" separation for Cr(VI) ions in wastewater.

2. Experimental

2.1 Reagents

Nylon membranes (0.45 μm) were purchased from the Shanghai Xingya factory. Potassium chromate (K_2CrO_4), methanol, ethanol, acetic acid, isopropanol, acetonitrile, ethyl acetate and petroleum ether were supplied by Fengchuan Chemical Reagent Co. Ltd, China. Dibenzoylmethane (DBM), allyl bromide (AB), ethylene glycol dimethacrylate (EDMA), and 2,2-azobisisobutyronitrile (AIBN) were obtained from Aladdin Reagent Co. Ltd, China. All reagents were of analytical grade, and deionized (DI) water was used in the experiments.

2.2 Synthesis of β-diketone functional monomers

Scheme 1 illustrates the procedure used for preparation of the β-diketone functional monomer 2-allyl-1,3-diphenyl-1,3-propanedione (ADPD). First, 20.0 mmol of dibenzoylmethane, 30.0 mmol of allyl bromide and 40 mmol of K_2CO_3 were added to a 100.0 mL round-bottom flask and dissolved in 60.0 mL of acetonitrile. The mixture was then added to a sealed reaction vial and allowed to react at room temperature for 36 h. Once the reaction was complete, as detected using thin layer chromatography (TLC), the mixture was transferred to a separating funnel and extracted using ethyl acetate (100 mL × 3). Following extraction, the mixture was washed in water (200 mL × 2) and dried under vacuum, and the organic phase was separated using silica gel column chromatography ($V_{PE} : V_{EA} = 10 : 1$, the volume ratio of petroleum ether to ethyl acetate) to obtain 4.28 g of yellowish target product with an 81% yield. (^{1}H NMR (600 MHz, $CDCl_3$) δ: 8.01–7.94 (m, 4H), 7.57 (ddt, 2H), 7.51–7.42 (m, 4H), 5.88 (ddt, 1H), 5.32 (t, 1H), 5.13–5.00 (m, 2H), 2.87 (tt, 2H); ^{13}C NMR (151 MHz, $CDCl_3$) δ: 195.29, 135.60, 134.79, 133.34, 128.64, 128.32, 117.00, 56.30, 33.28.)

2.3 Synthesis of ion-imprinted and non-imprinted composite membranes

IICMs were synthesized based on previous studies,[21,22] as follows: initially, appropriate quantities of K_2CrO_4 and ADPD (as listed in the ESI†) were dosed in conical flasks, and the corresponding solvents were added to react at 25 °C for 3 h, before adding the crosslinker (EDMA) and initiator (AIBN, 15.0 mg), and supplying nitrogen gas for 10 min to eliminate dissolved oxygen. The membranes were then immersed in the obtained pre-polymerization solution for 180 s, before being removed and sandwiched between two glass sheets for polymerization with thermal initiation at 60 °C for 24 h. Finally, Cr(VI) remaining in the imprinted composite membranes was removed using a mixture of methanol and acetic acid (9 : 1, v/v). The membranes were then further rinsed with methanol until they reached a pH of 7 and were finally vacuum dried to obtain the samples, labelled as Cr(VI)-IICM$_{1-11}$. As a control, corresponding non-imprinted composite membranes (NICM$_{1-11}$) were prepared and treated in a similar manner without the addition of Cr(VI).

2.4 Effect of synthesis ratio and solvents on adsorption capacity

The synthesis and performance of the imprinted system is affected by the type of solvent[23] and the amount of functional monomers[24] and crosslinkers[25,26] used. In addition, the structure of ADPD may vary between keto and enol forms under conditions of altered solvent polarity, which can impact the interactions between it and the template ions.[22,27] Therefore, in order to design IICMs with good recognition towards Cr(VI), a series of experiments were carried out using

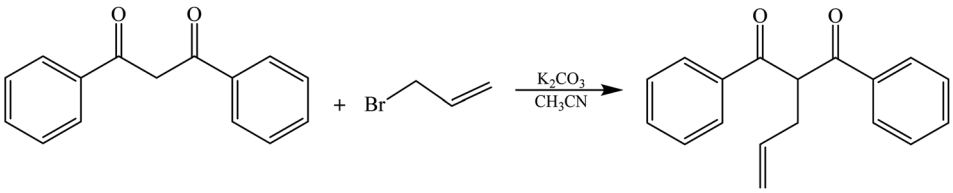

Scheme 1 Synthesis of 2-allyl-1,3-diphenyl-1,3-propanedione (ADPD).

different types of solvents and varying ratios of Cr(VI) to ADPD and EDMA.

2.5 Characterization

Absorption peaks of ADPD in various polar solvents and pH values were measured using a UV-visible (UV-Vis) spectrometer (UV 2550, Shimadzu, Japan). An attenuated total-reflective Fourier-transform infrared (ATR-FTIR) spectrometer (Nicolet 6700, Thermo Fisher, US) was used to characterize the chemical compositions of the membranes and record their absorption spectra within a wave number range of 4000–500 cm^{-1}. The membrane morphology was studied at an accelerated voltage of 15.0 kV using a field emission scanning electron microscope (FE-SEM) (Nano 450, Nova, USA) at magnifications of 10k and 20k. Platinum was applied to the membranes prior to analysis to obtain a better resolution and signal mass. The pore structures of the membranes were determined *via* nitrogen adsorption/desorption (Sorp-mini II, Microtrac, Japan) in conjunction with BET theory, and the specific surface areas, pore volumes, and average apertures of the membranes were calculated.

2.6 Adsorption experiments

2.6.1 Adsorption isotherms. Isothermal adsorption experiments[41,42] were carried out to test the performance of Cr(VI)-$IICM_{10}$ in removing Cr(VI) from aqueous solution. This was done by adding 20.0 mg of either $IICM_{10}$ or $NICM_{10}$ to 10 mL Cr(VI) solutions with different concentrations (in the range of 30–180 mg L^{-1}) which were then adsorption oscillated at 25 °C and pH = 5 for 8 h. All experiments were carried out three times in parallel to ensure reproducibility. The remaining Cr(VI) concentration in the solution was measured *via* UV-Vis photometry, allowing the equilibrium adsorption capacity, Q_e, to be calculated as follows:

$$Q_e = \frac{(C_0 - C_e) \times V}{M} \quad (1)$$

where C_0 and C_e are the initial and equilibrium concentrations of Cr(VI), respectively (mg L^{-1}), V is the volume of the solution (mL), and M is the mass (g) of the composite membrane.

2.6.2 Adsorption kinetics. The adsorption kinetics[43,45] of $IICM_{10}$ and $NICM_{10}$ towards Cr(VI) were studied through a series of experiments in which 20.0 mg of either Cr(VI)-$IICM_{10}$ or $NICM_{10}$ were added to 10 mL of 80 mg L^{-1} Cr(VI) at 25 °C to determine the concentrations of Cr(VI) ions in the adsorption solution over a time period ranging from 0.5–10 h.

2.6.3 Effect of pH and temperature on adsorption. The solution temperature[28,29] and pH[30] are essential factors impacts the recognition sites and adsorption capacity of the composite membranes. Further, the form which Cr(VI) ions take in solution depends on the pH value. More fundamentally, the structure of ADPD will be altered due to proton transfer at various pH values, which creates a level of response with pH and eventually causes a shift in the recognition sites of the imprinted composite membranes.[31] Thus, experiments were conducted to examine the impact on the absorption of Cr(VI) in solution of varying the pH from 1–11 and the temperature from 25–50 °C. The pH of the solution was regulated using HCl and NaOH, and the temperature was controlled using a water bath. Other conditions were as described in Section 2.6.1.

2.6.4 Selective adsorption experiment. Sequential permeation[44,45] properties of Cr(VI)-$IICM_{10}$ and $NICM_{10}$ were evaluated using an H-type permeation apparatus, as shown the ESI.† First, ionic solutions of Cr(VI), Cd(II), Cr(III) and HPO_4^{2-} (100 mg L^{-1}, 100 mL) were added to the left supply cell, and deionized water (100 mL) was added to the right cell as a receiving solution. An active membrane area of 1.54 cm^2 was employed, and the solution was maintained at 25 °C and pH = 5. Samples of the receiving cell were collected at different time points and the concentrations of the different ions in the permeate solution were recorded *via* ICP-OES, while ultimate data were averaged over three sets of parallel trials. Finally, the permeation, J, of the ions (mg h^{-1} cm^{-2}) was calculated as follows:

$$J_i = \frac{\Delta C_i V}{\Delta t A} \quad (2)$$

where the subscript i refers to either Cr(VI), Cr(III), Cd(II), Ni(II), or HPO_4^{2-}, $\Delta C_i/\Delta t$ is the average rate of change of the concentration of each ion in solution, V is the volume of receiving pool solution (mL), and A represents the effective area (cm^2).

2.6.5 Material reusability. To investigate the stabilization and reusability[44] of the Cr(VI)-$IICM_{10}$, five identical adsorption–desorption cycles were conducted using 50 mg of Cr(VI)-$IICM_{10}$ in 80 mg L^{-1} Cr(VI) at a pH of 5.0 over an adsorption time of 8 h. A methanol/acetic acid (9 : 1, v/v) solution was used to remove the Cr(VI) ions from the membrane after each cycle, which were then dried before being recycled. Each experiment was repeated three times to ensure repeatability.

Table 1 The effect of synthesis ratio and solvents on adsorption capacity

Solvent	Q_{IIP} (mg g^{-1})	Q_{NIP} (mg g^{-1})	α (Q_{IIP}/Q_{NIP})	Cr(VI) : ADPD : EDMA	Q_{IIP} (mg g^{-1})	Q_{NIP} (mg g^{-1})	α (Q_{IIP}/Q_{NIP})
CH_3OH	13.54	8.13	1.66	1 : 2 : 40	12.64	10.87	1.16
				1 : 4 : 40	21.54	12.91	1.67
CH_3CN	15.52	9.05	1.72	1 : 6 : 40	27.93	12.80	2.18
				1 : 8 : 40	19.01	15.76	1.21
CH_3CH_2OH	27.93	12.80	2.18	1 : 6 : 10	18.18	16.05	1.13
				1 : 6 : 20	22.44	14.57	1.54
$(CH_3)_2CHOH$	19.61	9.75	2.01	1 : 6 : 30	30.35	11.23	2.70
				1 : 6 : 50	17.69	13.38	1.32

3. Results and discussion

3.1 Effect of synthesis ratio and solvents on adsorption capacity

Table 1 shows that there are noticeable differences in the adsorbed amounts of Cr(VI) for the membranes synthesized using different component ratios, with the Cr(VI)-IICM$_{10}$ membrane (Cr(VI) : ADPD : EDMA ratio of 1 : 6 : 30) having the highest adsorption capacity of up to 30.35 mg g^{-1}, as well as the highest imprinting factor, α, of 2.70. On the other hand, the solvent polarity[32] also has an impact on adsorption of composite membranes, with the loading and selectivity towards Cr(VI) in the IICMs obtained using weakly polar solvents (*e.g.* ethanol, isopropanol) being significantly better than those of the membranes obtained using strongly polar solvents (*e.g.* methanol, acetonitrile). This may be attributed to ADPD undergoing structural interconversion in weakly polar solvents, and creating more coordination groups (such as –OH, C=O, C=C and α-H) in solution,[33] which reinforced the imprinting of Cr(VI) during the preparation of the IICMs. These results are consistent with the UV-Vis absorption spectra of ADPD under different solvent polarity conditions (Fig. 1).

3.2 Characteristics

3.2.1 UV-Vis spectra. UV-Vis spectra of ADPD (Fig. 1) were acquired to determine its responsiveness to variations in solvent polarity and pH. The solvents used included methanol, acetonitrile, isopropanol, and ethanol, with polarities of 6.6, 6.2, 4.4, and 4.3, respectively. The results show that ADPD contains primarily diketone structures (C=O, ~280 nm) under more polar solvents. In contrast, enol structures (=C–OH, ~245 nm) were noticeably increased in the lower polarity solvents.[34] This is likely due to the formation of intramolecular hydrogen bonds from carbonyl groups within the diketone structures of ADPD in polar solvents, which increases their stability.[35,36]

3.2.2 ATR-FTIR. The surface contents of ADPD, nylon membranes, Cr(VI)-IICM$_{10}$, and NICM$_{10}$ were analyzed using ATR-FTIR (Fig. 2). An intense and sharp peak at ~1690 cm^{-1} was observed in the spectrum for ADPD, which corresponds to superposition with stretching vibrations of C=O and C=C, while those observed from ~1585–1440 cm^{-1} are associated with the skeletal vibrations of aromatic rings and the bending vibrations of –CH$_2$. Additionally, the stretched vibrations of –CH$_2$ and the =C–H stretched vibrational peaks of aromatic rings (olefins) were observed at 2935 cm^{-1} and 3080 cm^{-1}, respectively.

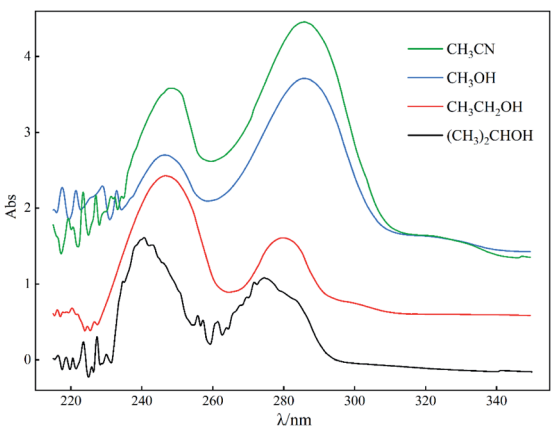

Fig. 1 UV-Vis spectra of 0.1 mmol L^{-1} ADPD for different polarities of solvents.

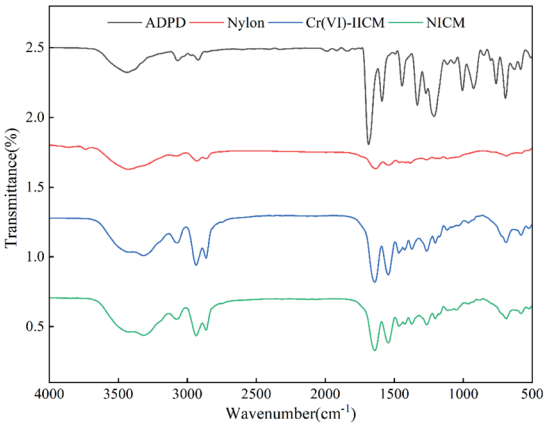

Fig. 2 ATR-FTIR spectra of the functional monomer (ADPD) and the nylon, Cr(VI)-IICM$_{10}$, and NICM$_{10}$ membranes.

As expected, all of characteristic peaks from ADPD were also observed in the Cr(VI)-IICM$_{10}$ and NICM samples but not in the primary nylon membranes. In the spectra for Cr(VI)-IICM$_{10}$ and NICM$_{10}$, novel peaks located at 1460 cm^{-1} and 1545 cm^{-1} were attributed to the –CH$_2$ and C=C groups of the aromatic ring, respectively, while the absorption peaks at 2940 and 3075 cm^{-1} are attributed to the bending vibrations of methylene (–CH$_2$) and the stretching vibrations of aromatic rings (olefins, =C–H), respectively. It is important to mention that a fresh absorption peak positioned at ~1645 cm^{-1} in the Cr(VI)-IICM$_{10}$ and NICM$_{10}$ spectra was attributed to the stretching vibrations of the carbonyl group (C=O). These results confirm that ADPD was successfully introduced to the nylon membrane substrate, and that ion-imprinted layers of Cr(VI) were subsequently formed on the membrane surface.

3.2.3 FE-SEM. The morphologies of the nylon, Cr(VI)-IICM$_{10}$, and NICM$_{10}$ membranes were further analyzed using FE-SEM. As shown in Fig. 3, the image as a whole shows a certain aperture structure. It is evident from these images that the structure of the composite membrane changed significantly compared to the smooth and porous surface of the original nylon membrane (Fig. 3(a)), which presented a rough and tight shape, with a covered and filled porous structure. This difference may be attributed to the imprinting process, which forms a thin and dense layer on the surface of the nylon membranes. Compared to the NICM (Fig. 3(c)), the surface and intrapore imprinting layers of membranes were significantly increased after the addition of Cr(VI) (Fig. 3(b)), indicating successful preparation of the designed Cr(VI)-IICM$_{10}$ membrane.

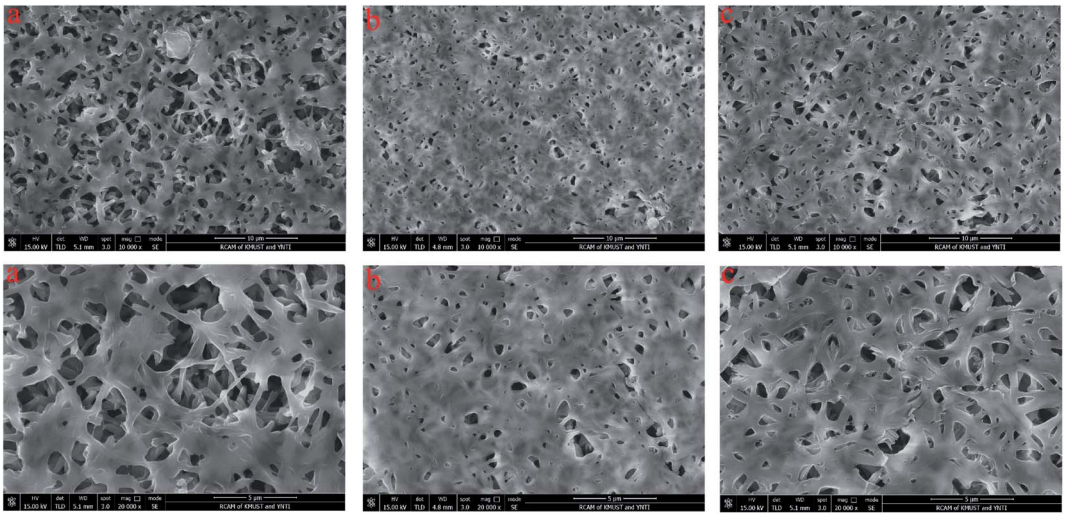

Fig. 3 FE-SEM images showing the morphological structures of the (a) nylon, (b) Cr(VI)-IICM$_{10}$, and (c) NICM$_{10}$ membranes.

3.2.4 BET. Isothermal adsorption/desorption curves of the nylon, Cr(VI)-IICM$_{10}$, and NICM$_{10}$ membranes are shown in the ESI,† whence it can be seen that the isothermal adsorption/desorption curves of NICM$_{10}$ and nylon were similar, indicating that their surface structures are analogous, while those of Cr(VI)-IICM$_{10}$ were somewhat different. These measurements were used to calculate the surface areas, pore sizes, and pore volumes of the three membranes (Table 2), which showed that all three membranes had an average pore size of 2–50 nm, indicating that they were mesoporous.

However, in contrast with the nylon membranes, the specific surface area, hole volume, and aperture of the composite membranes was significantly reduced, and this reduction was significantly greater for Cr(VI)-IICM$_{10}$ compared to NICM$_{10}$. This may be due to the former having a large, layered imprint structure on its surface, while the latter only possesses a small polymer covering. These results are consistent with the FE-SEM images (Fig. 3), which indicates that a large number of identification site structures were successfully formed on the membrane surface.

3.3 Adsorption experiments

3.3.1 Adsorption isotherms. Adsorption isotherms of Cr(VI)-IICM$_{10}$ and NICM$_{10}$ were studied in detail. As Fig. 4 shows, the binding capacities of both Cr(VI)-IICM$_{10}$ and NICM$_{10}$ were positively correlated with the initial solution concentration of Cr(VI). In addition, the maximum adsorption capacity of Cr(VI)-IICM$_{10}$ (29.66 mg g^{-1}) was higher than that of NICM$_{10}$, which may be attributed to the fact that the imprinted layer in the former IICM$_{10}$ endows it with a number of rich micropores and high-affinity recognition cavities, which is not the case with NICM$_{10}$. Finally, the adsorption characteristics of Cr(VI)-IICM$_{10}$ and NICM$_{10}$ were researched with Langmuir and Freundlich isotherm models.

$$Q_e = \frac{K_L Q_m C_e}{1 + K_L C_e} \quad (3)$$

$$Q_e = K_F C_e^{1/n} \quad (4)$$

where Q_e is the equilibrium adsorption capacity of Cr(VI) (mg g^{-1}), Q_m is the theoretical maximum adsorption capacity of Cr(VI) (mg g^{-1}), C_e is the equilibrium concentration of Cr(VI) in solution (mg L^{-1}), and K_L and K_F are the Langmuir and Freundlich constants, respectively.

Table 2 Surface area, pore size, and pore volume of the nylon, Cr(VI)-IICM$_{10}$, and NICM$_{10}$, membranes

Membranes	Surface area (m^2 g^{-1})	Pore volume (cm^3 g^{-1})	Pore size (nm)
Nylon	10.282	0.0373	14.525
NICM$_{10}$	9.233	0.0243	10.537
Cr(VI)-IICM$_{10}$	7.817	0.0168	8.618

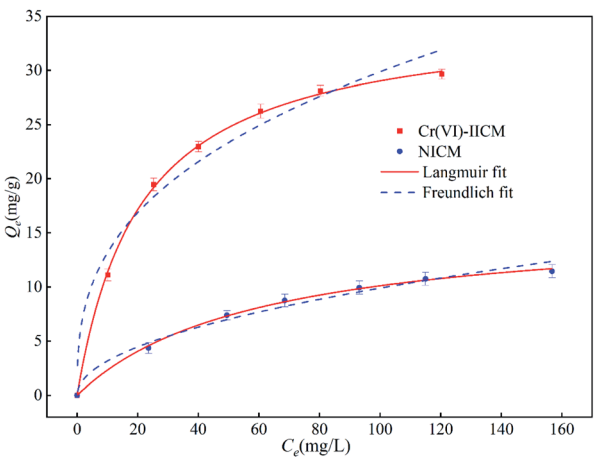

Fig. 4 Adsorption isotherms for Cr(VI)-IICM$_{10}$ and NICM$_{10}$, along with Langmuir and Freundlich fitting curves for Cr(VI)-IICM$_{10}$ and NICM$_{10}$.

Table 3 Correlation parameters of the Langmuir and Freundlich fitting curves for Cr(VI)-IICM$_{10}$ and NICM$_{10}$

Isotherm model		Langmuir			Freundlich		
	Q_e (mg g^{-1})	K_L	Q_m (mg g^{-1})	R^2	K_F	$1/n$	R^2
Cr(VI)-IICM$_{10}$	29.66	0.0475	35.13	0.9985	5.813	0.3560	0.9562
NICM$_{10}$	11.47	0.0169	16.17	0.9959	1.012	0.4935	0.9815

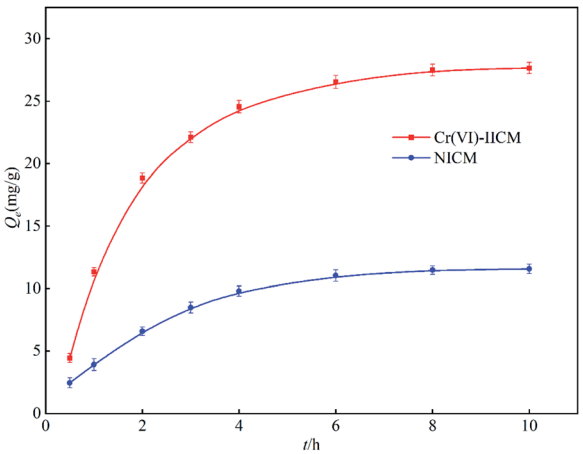

Fig. 5 The kinetic adsorption curves of Cr(VI)-IICM$_{10}$ and NICM$_{10}$.

The fitting parameters of the Langmuir and Freundlich isotherms are shown in Table 3, which reveals that the correlation coefficient of Cr(VI)-IICM$_{10}$ in the Langmuir model (R^2 = 0.9985) is better than that of the Freundlich model (R^2 = 0.9562), indicating that distribution of adsorption sites is uniform, and that monolayer adsorption occurs.

3.3.2 Adsorption kinetics. Dynamic adsorption experiments were carried out on Cr(VI)-IICM$_{10}$ and NICM$_{10}$ to study the kinetics of the adsorption process. Fig. 5 shows that the adsorption capacity of Cr(VI)-IICM$_{10}$ reached 80% of the total capacity in the first 3 h of adsorption, which is due to the imprinted composite membrane having sufficient binding sites, as well as to the strong chelation between dicarbonyl and Cr(VI). Eventually, the adsorbed Cr(VI) occupies most of the binding sites, and reaches equilibrium after 8 h. However, for NICM$_{10}$, the lack of Cr(VI) imprint steps during pore formation meant that there were no specific interactions between Cr(VI) and ADPD, resulting in a relatively slow adsorption rate of NICM$_{10}$ on Cr(VI) is. These results clearly show that the imprinting effect greatly increases the adsorption capacity of Cr(VI)-IICM$_{10}$ towards Cr(VI) relative to NICM$_{10}$.

Experimental data were fitted using the pseudo-first-order and pseudo-second-order adsorption kinetic models, as follows:

$$\ln(Q_e - Q_t) = \ln Qe - k_1 t \quad (5)$$

$$\frac{t}{Q_t} = \frac{1}{k_2 Q_e^2} - \frac{t}{Q_e} \quad (6)$$

where Q_e (mg g^{-1}) is the equilibrium adsorption capacity of Cr(VI), Q_t (mg g^{-1}) is adsorption capacity under different contact times, t, and k_1 (min^{-1}) and k_2 (g mg^{-1} min^{-1}) are the pseudo first- and pseudo-second-order model constants, respectively.

The adsorption of Cr(VI) on Cr(VI)-IICM$_{10}$was analyzed, and the results are shown in Fig. 6. It is evident that the correlation coefficient of the pseudo first-order equation (R^2 = 0.9960) was larger than that of the pseudo-second-order equation (R^2 = 0.7544), indicating that the adsorption of Cr(VI) follows pseudo first-order kinetics.

3.3.3 Effect of pH and temperature on adsorption. Results for the adsorption capacity of Cr(VI)-IICM$_{10}$ as a function of temperature are shown in Fig. 7(a). It is evident that as temperature increases, the adsorption of Cr(VI)on the membrane surface weakens. This is likely because the Cr(VI) ions move faster at higher temperatures, making it more difficult to be bound by the membrane. Additionally, the elevated temperatures might induce a gradual conversion of ADPD from enolic to ketonic structures,[36]

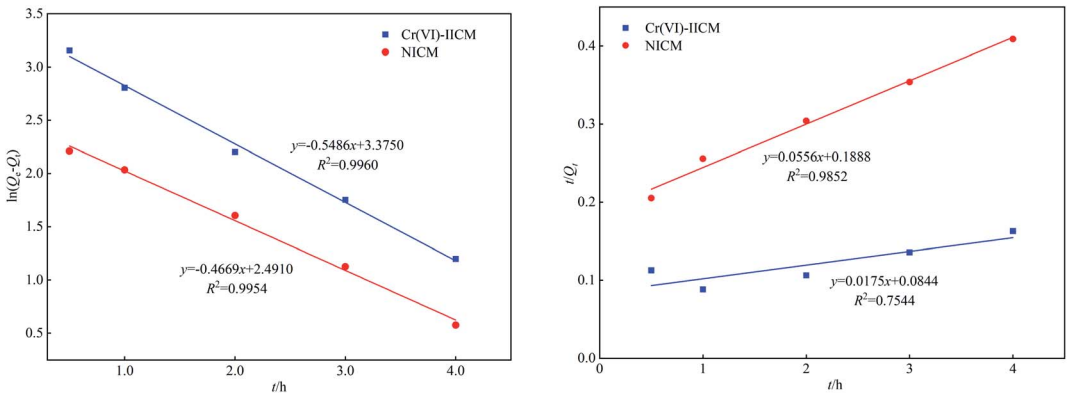

Fig. 6 Pseudo-first- and pseudo-second-order kinetic fitting curves for Cr(VI)-IICM$_{10}$ and NICM$_{10}$.

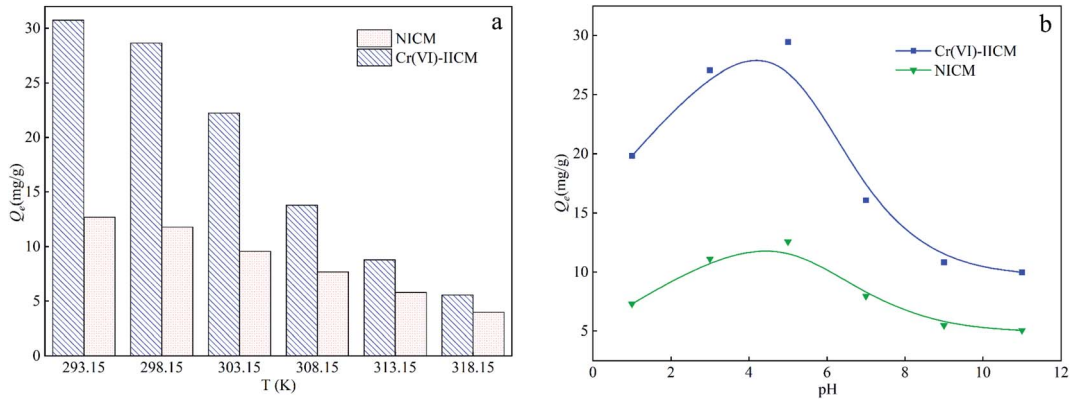

Fig. 7 Effect of (a) temperature and (b) pH on adsorption performance of Cr(VI)-IICM$_{10}$ and NICM$_{10}$.

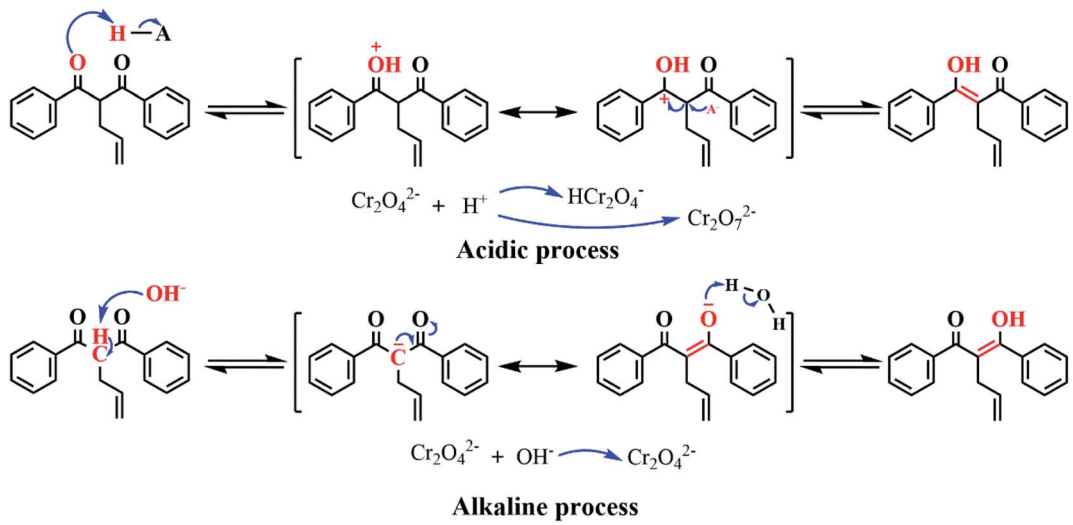

Fig. 8 Mechanism of the structural variations of ADPD under acidic or basic conditions.

which is unfavorable for the adsorption of Cr(VI) upon Cr(VI)-IICM$_{10}$. Taking into consideration the real-world application of IICMs and local climatic environments, subsequent experiments were carried out at 25 °C.

Fig. 7(b) shows that the adsorption capacity of both Cr(VI)-IICM$_{10}$ and NICM$_{10}$ towards Cr(VI) did vary modestly with the solution pH, with the former having a higher adsorption capacity at all pH values. In particular, the amount of Cr(VI) adsorbed on Cr(VI)-IICM$_{10}$ was roughly twofold that on NICM$_{10}$ at pH 5 owing to the imprinting of the Cr(VI) selective-recognition cavities. The Cr(VI) absorption capacity increased markedly from pH 1–5 and decreased significantly thereafter. A possible explanation for this is that ADPD produced enol anions (C=C–O–) under alkaline conditions, which is not conducive to the adsorption of chromate ions (CrO_4^{2-}) on composite membranes (Fig. 8).[22,39]

Under acidic conditions (pH < 7), ADPD is promoted to generate enol cations (C–C=OH^+),[37] thus achieving greater adsorption capacity towards CrO_4^{2-}. However, in strongly acidic solutions (pH < 3), the adsorption ability of composite membranes towards Cr(VI) was substantially reduced. It is believed that ADPD tends to form ketonic structures (C=O) in stronger acidic environments, which causes a reduction of enol

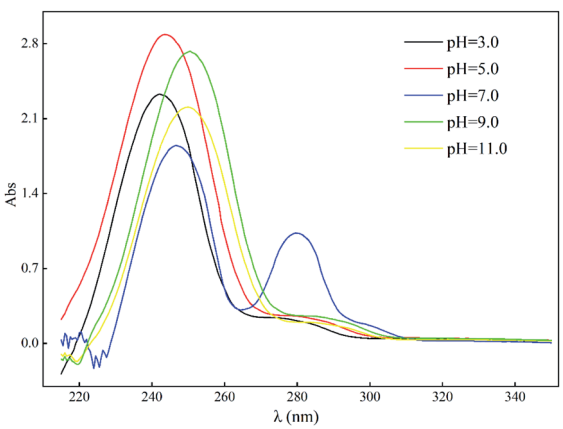

Fig. 9 UV-Vis spectra of ADPD solutions (0.1 mmol L^{-1}, ethanol) with various pH values.

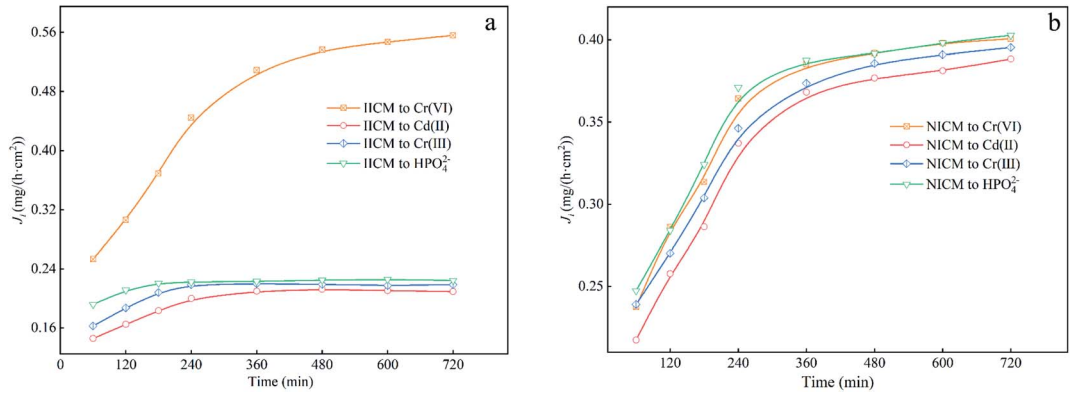

Fig. 10 Selective permeation properties of (a) Cr(VI)-IICM$_{10}$ and (b) NICM$_{10}$ towards Cr(VI), Cd(II), Cr(III), and HPO_4^{2-}.

cations (C–C=OH$^+$) in the solution and eventually reduces the adsorption capacity of composite membranes (Fig. 8). These results demonstrate that Cr(VI)-IICM$_{10}$ is pH-responsive and can potentially act as a "smart membrane" to control both the separation and enrichment of Cr(VI) from solutions.

Fig. 9 shows that the changes of ADPD in solution with different pH. In a neutral medium, ADPD exhibited both ketone and enol structures and possesed two absorption peaks in the UV-Vis spectrogram; however, as the solution changed to basic or acidic, the carbonyl (C=O) absorption peak at 280 nm decreased substantially, which indicates that the diketone structures of ADPD were converted to enols.[37] Further, as the acidity of the solution increased, the enolic structures of ADPD further decreased, which indicates that ADPD exists primarily as keto structures in more strongly acidic and basic solutions.[38]

These results indicate that the β-diketone functional monomer (ADPD) switches between ketone and enol in response to variations in the pH of the matrix solution. Hence, this monomer can be utilized for the generation of pH-responsive IICMs (*e.g.* Cr(VI)-IICM$_{10}$) capable of achieving pH-controlled and selective separation of Cr(VI) in solution.

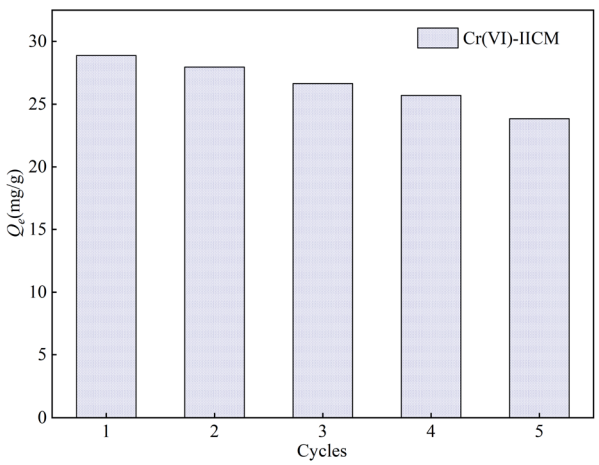

Fig. 11 Stability and regenerative capacity of Cr(VI)-IICM$_{10}$ after repeated adsorption–desorption cycles.

3.3.4 Selective permeation of composite membrane. Fig. 10 shows selective osmosis curves of Cr(VI)-IICM$_{10}$ and NICM$_{10}$ with respect to four different metal ions (Cr(VI), Cd(II), Cr(III) and HPO_4^{2-}). As Fig. 11(a) shows, the permeation curves for Cr(VI)-IICM$_{10}$ reveal a far greater permeation capacity towards Cr(VI) than the other three ions, which means that Cr(VI)-IICM$_{10}$ was able to maintain high selectivity towards Cr(VI) even in the presence of other ions. This is likely due to the fact that the imprinted layer specifically targets Cr(VI), while no specific recognition sites were present for the competing ions. However, Fig. 10(b) shows that the permeation curves of the different ions on NICM$_{10}$ were very similar to each other both in terms of values and the underlying trends. A comparison of the results between Fig. 10(a) and (b) illustrates that Cr(VI)-IICM$_{10}$ maintains a selective and excellent permeation separation performance towards Cr(VI) the presence of other ions.

3.3.5 Reusability of Cr(VI)-IICM$_{10}$. Reusability[45] is crucial to the real-world application of IICMs. Fig. 11 shows that the adsorption capacity of Cr(VI)-IICM$_{10}$ towards Cr(VI) decreased by ~17.5% after five adsorption/desorption cycles. Also combination ability of Cr(VI)-IICM$_{10}$ without a obvious reduction, adsorption capacity still maintained a reasonable level. These results demonstrate that the Cr(VI)-IICM$_{10}$ membrane can be reused multiple times with outstanding stability and regeneration performance.

4. Conclusions

In this study, a novel ion-imprinted composite membrane (IICM) was successfully developed for the selective separation and rapid identification of Cr(VI) in solution. This was achieved using Cr(VI) as template ions alongside a customized β-diketone functional monomer (ADPD) in a combined ion surface imprinting and membrane separation technique. ATR-FTIR analysis revealed that ADPD was strongly grafted to the nylon membrane, while FE-SEM and BET further confirmed that an imprinted layer structure of Cr(VI) was formed on the Cr(VI)-IICM$_{10}$ membrane. Further, UV-Vis and adsorption experiments indicated that Cr(VI)-IICM$_{10}$ underwent structural changes in response to shifts in the pH, and also exhibited a high adsorption capacity towards Cr(VI) with a maximum

value of 30.35 mg g^{-1}. The adsorption rate was consistent with pseudo-first-order kinetics, and the equilibrium adsorption showed a good fit with Langmuir isotherms. Overall, Cr(VI)-$IICM_{10}$ also exhibited remarkable osmotic selectivity, with permeation of Cr(VI) ($J_i = 0.556$) far higher than those of three competing ions ($J_i \approx 0.217$), and showed excellent stability and reusability after five adsorption–desorption cycles. These results strongly suggest that the use of ADPD to fabricate IICMs is a cost-effective and convenient separation strategy, which holds promise as a reliable and controlled approach for the selective enrichment and separation of Cr(VI) from aqueous solution.

Conflicts of interest

There are no conflicts to declare.

Acknowledgements

The work was supported by the National Natural Science Foundation of China (grant numbers 21764008).

References

1 X. H. Yuan, N. D. Xue and Z. G. Han, *J. Environ. Sci.*, 2021, **101**, 217–226.
2 G. W. Qin, Z. D. Niu, J. D. Yu, Z. H. Li, J. Y. Ma and P. Xiang, *Chemosphere*, 2021, **267**, 129205.
3 K. H. Cheung and J. D. Gu, *Int. Biodeterior. Biodegrad.*, 2007, **59**, 8–15.
4 T. Pavesi and J. C. Moreira, *J. Appl. Toxicol.*, 2020, **40**, 1183–1197.
5 T. L. DesMarais and M. Costa, *Curr. Opin. Toxicol.*, 2019, **14**, 1–7.
6 S. Y. Guo, C. Q. Xiao, N. Zhou and R. Chi, *Environ. Chem. Lett.*, 2021, **19**, 1413–1431.
7 B. Verma and C. Balomajumder, *Bull. Chem. Soc. Ethiop.*, 2020, **34**, 67–74.
8 Y. A. El-Taweel, E. M. Nassef, I. Elkheriany and D. Sayed, *Egypt. J. Pet.*, 2015, **24**, 183–192.
9 C. Pan, L. D. Troyer, J. G. Catalano and D. E. Giammar, *Environ. Sci. Technol.*, 2016, **50**, 13502–13510.
10 Y. Q. Xing, X. M. Chen and D. H. Wang, *Environ. Sci. Technol.*, 2007, **41**, 1439–1443.
11 A. S. Dharnaik and P. K. Ghosh, *Environ. Technol.*, 2014, **35**, 2272–2279.
12 J. T. Liu, W. D. Zhang, Z. Q. Ren and J. A. Ma, *Ind. Eng. Chem. Res.*, 2009, **48**, 4500–4506.
13 S. Caprarescu, R. G. Zgarian, G. T. Tihan, V. Purcar, E. E. Totu, C. Modrogan, A. L. Chiriac and C. A. Nicolae, *Polymers*, 2020, **12**, 1792.
14 M. Bodzek, *Ecol. Chem. Eng. S*, 2013, **20**, 633–658.
15 S. Sharma and A. Bhattacharya, *Appl. Water Sci.*, 2017, **7**, 1043–1067.
16 S. S. Kerur, S. Bandekar, M. S. Hanagadakar, S. S. Nandi, G. M. Ratnamala and P. G. Hegde, *Mater. Today*, 2021, **42**, 1112–1121.
17 J. J. Wang, Y. J. Han, J. Li and J. Wei, *Sep. Purif. Technol.*, 2017, **177**, 62–70.
18 Z. Q. Ren, X. Y. Zhu, J. Du, D. L. Kong, N. Wang, Z. Wang, Q. Wang, W. Liu, Q. S. Li and Z. Y. Zhou, *Appl. Surf. Sci.*, 2018, **435**, 574–584.
19 D. S. Sun, M. J. Meng, Y. Qiao, Y. H. Zhao, Y. S. Yan and C. X. Li, *Sep. Purif. Technol.*, 2018, **194**, 64–72.
20 J. Zhang, R. Wang, X. Ou, X. Zhang, P. Liu, Z. Chen, B. Zhang, C. Liu, S. Zhao, Z. Chen, J. Zhu, S. Lu and P. Zhang, *Sep. Purif. Technol.*, 2021, **259**, 118165.
21 Y. M. Liu, D. Q. Hu, X. Z. Hu, S. L. Chen, L. Zhao, Y. L. Chen, P. Yang, X. C. Qin, H. L. Cheng and F. T. Zi, *Anal. Lett.*, 2020, **53**, 1113–1139.
22 H. L. Cheng, X. F. Zhu, S. X. Yang, Y. X. Wu, Q. Cao and Z. T. Ding, *J. Appl. Polym. Sci.*, 2013, **128**, 363–370.
23 W. Meouche, K. Laatikainen, A. Margaillan, T. Silvonen, H. Siren, T. Sainio, I. Beurroies, R. Denoyel and C. Branger, *Eur. Polym. J.*, 2017, **87**, 124–135.
24 J. L. Urraca, M. C. Carbajo, M. J. Torralvo, J. Gonzalez-Vazquez, G. Orellana and M. C. Moreno-Bondi, *Biosens. Bioelectron.*, 2008, **24**, 155–161.
25 K. Yoshimatsu, T. Yamazaki, I. S. Chronakis and L. Ye, *J. Appl. Polym. Sci.*, 2012, **124**, 1249–1255.
26 H. Q. Hu, Z. Ren, Y. Xi, L. L. Fang, D. F. Fang, L. M. Yang, P. H. Shao, H. Shi, K. Yu and X. B. Luo, *Chem. Eng. J.*, 2021, **420**, 129611.
27 E. V. Sergeeva, L. N. Puntus, F. Kajzar, I. Rau, B. Sahraoui, I. S. Pekareva, K. Y. Suponitsky, I. S. Bushmarinov and K. A. Lyssenko, *Opt. Mater.*, 2013, **36**, 47–52.
28 J. Li, F. Ji, D. H. L. Ng, J. Liu, X. M. Bing and P. Wang, *Chem. Eng. J.*, 2019, **369**, 611–620.
29 J. S. Cao, X. D. Wu, L. T. Wang, G. S. Shao, B. Y. Qin, Z. H. Wang, T. Wang and Y. J. Fu, *Int. J. Biol. Macromol.*, 2021, **181**, 1231–1242.
30 L. P. Zhao, L. S. Li, C. Zhu, M. Ghulam and F. Qu, *Anal. Chim. Acta*, 2020, **1097**, 161–168.
31 D. Wu, X. Fang, J. Song, L. Qu, X. Zhou, H. Xiang, J. Wang and J. Liu, *Dyes Pigm.*, 2021, **184**, 108851.
32 I. E. Charif, S. M. Mekelleche and D. Villemin, *J. Theor. Comput. Chem.*, 2010, **9**, 1021–1032.
33 S. K. Wu, G. S. Dai, L. S. Liu and J. K. Chang, *Polym. Degrad. Stab.*, 1986, **16**, 169–186.
34 J. Zawadiak and M. Mrzyczek, *Spectrochim. Acta, Part A*, 2010, **75**, 925–929.
35 K. R. Wursthorn and E. H. Sund, *J. Heterocycl. Chem.*, 1972, **9**, 25–29.
36 J. Zhao, J. Zhao, X. He, Z. Tan, X. Cheng, Q. Han and C. Zhou, *J. Mater. Chem. C*, 2021, **9**, 1000–1007.
37 N. D. Tivendale, N. W. Davies, J. Horne, J. J. Ross and J. A. Smith, *Aust. J. Chem.*, 2015, **68**, 345–348.
38 L. Zhang, J. Zhang, Z. J. Li, Y. Y. Qin, Q. P. Lin and Y. G. Yao, *Chem.–Eur. J.*, 2009, **15**, 989–1000.
39 A. A. Adeniyi and J. Conradie, *Electrochim. Acta*, 2019, **297**, 947–960.
40 J. Q. Fu, L. X. Chen, J. H. Li and Z. Zhang, *J. Mater. Chem. A*, 2015, **3**, 13598–13627.

41 X. Q. Cai, J. H. Li, Z. Zhang, F. F. Yang, R. C. Dong and L. X. Chen, *ACS Appl. Mater. Interfaces*, 2014, **6**, 305–313.
42 S. F. Xu, L. X. Chen, J. H. Li, Y. F. Guan and H. Z. Lu, *J. Hazard. Mater.*, 2012, **237**, 347–354.
43 L. Y. Wang, J. H. Li, J. N. Wang, X. T. Guo, X. Y. Wang, J. Choo and L. X. Chen, *J. Colloid Interface Sci.*, 2019, **541**, 376–386.
44 J. Lu, Y. Y. Qin, Y. L. Wu, M. J. Meng, Y. S. Yan and C. X. Li, *Environ. Sci. Water Resour.*, 2019, **5**, 1626–1653.
45 Y. A. B. Neolaka, Y. Lawa, J. N. Naat, A. A. P. Riwu, H. Darmokoesoemo, G. Supriyanto, C. I. Holdsworth, A. N. Amenaghawon and H. S. Kusuma, *React. Funct. Polym.*, 2020, **147**, 104451.